The electronic structure of PdO found by photoemission (UPS and XPS) and inverse photoemission (BIS)

1997 J. Phys.: Condens. Matter 9 3987

(http://iopscience.iop.org/0953-8984/9/19/018)

J. Phys.: Condens. Matter **9** (1997) 3987–3999. Printed in the UK PII: S0953-8984(97)80440-7

The electronic structure of PdO found by photoemission (UPS and XPS) and inverse photoemission (BIS)

Th Pillo†, R Zimmermann, P Steiner and S Hüfner

Institut für Experimentalphysik, Universität des Saarlandes, D-66041 Saarbrücken, Germany

Received 23 December 1996

Abstract. The electronic structure of the 4d transition-metal oxide PdO is investigated by photoemission (UPS and XPS), inverse photoemission (BIS; $h\nu = 1486.6$ eV), and electron energy loss spectroscopy in reflection geometry (REELS; primary energy, 50 eV$\leqslant E_0 \leqslant$ 1500 eV). The valence band spectra are compared to recent theoretical *ab initio* band-structure calculations. Good agreement between theory and experiment is found in the occupied part of the band structure down to 8 eV below E_F as well as in the unoccupied part up to 6 eV above E_F. This confirms the common view that the electronic structure of the 4d transition-metal oxides, e.g. PdO, can be explained in terms of a single-electron picture. Nevertheless correlation effects among the Pd 4d electrons are clearly visible in the spectra, as e.g. satellites of the Pd core level spectra. In order to explain the origin of these satellites we performed simple cluster model calculations and as a result we can explain one satellite in a screening picture by means of a charge transfer process. In addition radiation damage effects in PdO during the electron bombardment in the BIS experiments are reported. This is explained by the formation of the Pd $4d^{10}$-like states connected with oxygen loss due to the electron bombardment.

1. Introduction

The nonmagnetic transition-metal oxides (TMOs) PdO and PtO are well known as catalyst materials especially in motor industry. PdO, as a representative of a 4d TMO, is a p semiconductor. It crystallizes in the tetragonal cooperite structure (space group D_{4h}^9) [1, 2]. During the last few decades there has been a strong interest in the investigation of the electronic structure of 3d TMOs because here the localized character of the 3d electrons leads to strong correlation effects and therefore single-electron band-structure calculations are only of limited value for the explanation of their electronic properties. For example the electronic structure of the prototype material NiO is not understood even now [3]. This also holds for the high-temperature superconductors (HTSCs) where electron–electron correlations in the CuO_2 planes play a crucial role.

PdO is the 4d counterpart of NiO, both having a formal d^8 occupation in the ground state. Unfortunately there is only a little published work on the electronic structure of bulk PdO, whereas the chemisorption of oxygen on Pd single crystals has been investigated in detail [4, 5]. Theoretical band-structure calculations of PdO and PtO within the local-density approximation (LDA) have been presented recently [6–8] but to our knowledge only the paper of Holl *et al* [9] deals with the experimentally derived electronic structure of PdO.

† Present address: Université de Fribourg, Institut de Physique, CH-1700 Fribourg, Switzerland. e-mail: thorsten.pillo@unifr.ch

0953-8984/97/193987+13$19.50

Due to the more delocalized nature of the d orbitals in the 4d TMOs as compared to the 3d TMOs electron–electron correlations should be small in the former. Therefore Brandow and Goodenough [10, 11] proposed that the lower symmetric tetragonal structure in these compounds is favoured because of the possibility of building up the band gap by crystal field splitting of the 4d electrons only, that is within a pure one-electron picture, but this point and the magnitude of the gap itself have remained unclear until now. While the calculations revealed for the gap a value of 0.1 eV or even semi-metallic behaviour [6, 8] the spread of the experimental results ranges from 0.8 eV up to 2.6 eV [1, 7, 12–15].

Here we present experimental results from photoemission (UPS and XPS), inverse photoemission (BIS), and electron-energy loss spectroscopy in reflection geometry (REELS). After having given some experimental details the valence band structure obtained from UPS (He-I and He-II) and XPS (monochromatized Al Kα radiation) is compared to available theoretical results. The unoccupied part of the band structure is compared to the BIS experiments. These data together with the REELS data are used to extract the magnitude of the band gap. In the last part we present some data which show that PdO is unstable when annealed under UHV conditions and especially under electron bombardment with high current densities as in the BIS experiments.

2. Experimental details

The data are collected in a VG-Escalab MK II spectrometer equipped with a twin anode delivering Al Kα and Mg Kα radiation (1486.6 and 1253.6 eV respectively) and a gas discharge lamp for the He-I and He-II measurements (21.2 and 40.8 eV respectively). The energy resolution depends on the conditions of the spectrometer and is at its best 0.8 eV for XPS and 0.03 eV for UPS. In addition a monochromatized Al Kα source gives high energy resolution for XPS of 0.5 eV. Combined with a high-current electron gun (about 100 μA sample current) BIS experiments with a resolution of 0.8 eV can be performed. The same electron gun is at lower currents (1–20 nA) used for REELS experiments with primary electron energies from 50 eV up to 1500 eV with an energy resolution of about 0.35 eV.

Samples of PdO were prepared according to well known procedures for the formation of PdO [12]. Thin polycrystalline Pd foils of high purity (99.9%) were polished and cleaned *in situ* by Ar etching. Oxidation was performed in a gas cell connected to the spectrometer at 5 bar oxygen at about 550 °C for about 4 h. For comparison one sample was prepared outside the spectrometer in a furnace at 550 °C in 1 bar oxygen for 24 h. This metal foil was covered with a blue–green PdO film, sometimes with a black tinge. This sample was cleaned by etching with oxygen and reoxidized *in situ*. Both procedures gave the same XPS–UPS data but since the film first oxidized outside the spectrometer was thicker and more stable (see below) the data presented here are from this film. Furthermore a PdO pellet was prepared from commercially available PdO powder and cleaned by *in situ* scraping. Due to the porous nature this pellet showed a large amount of carbon contamination. The XPS results for this pellet agreed with those of the films. Because of the large contaminations reliable UPS, BIS, and REELS data could not be obtained, but a part of the pellet was checked with x-ray diffraction whereby no phases other than PdO could be detected. In table 1 we show the binding energies for the Pd 3d doublet in comparison to other data.

It should be mentioned here that the PdO samples were not stable in UHV under XPS for longer periods, when a small loss of oxygen could be determined by XPS. The samples were then reoxidized by first sputtering with oxygen followed by *in situ* reoxidization.

Table 1. A compilation of the Pd 3d binding energies for Pd metal and PdO from this work compared to published data. Note the rather good coincidence in particular for the chemical shift.

Pd $3d_{5/2}$ metal (eV)	Pd $3d_{3/2}$ metal (eV)	Pd $3d_{5/2}$ PdO (eV)	Pd $3d_{3/2}$ PdO (eV)	ΔE_{chem} (eV)	Reference
335.2	340.5	336.7	342.0	1.50	this work
334.4	339.5	335.7	341.2	1.55	[16]
335.1	340.3	336.5	341.9	1.60	[17]
335.4	340.4	337.0	342.2	1.65	[18]
335.0	341.2	336.3	342.5	1.30	[19]

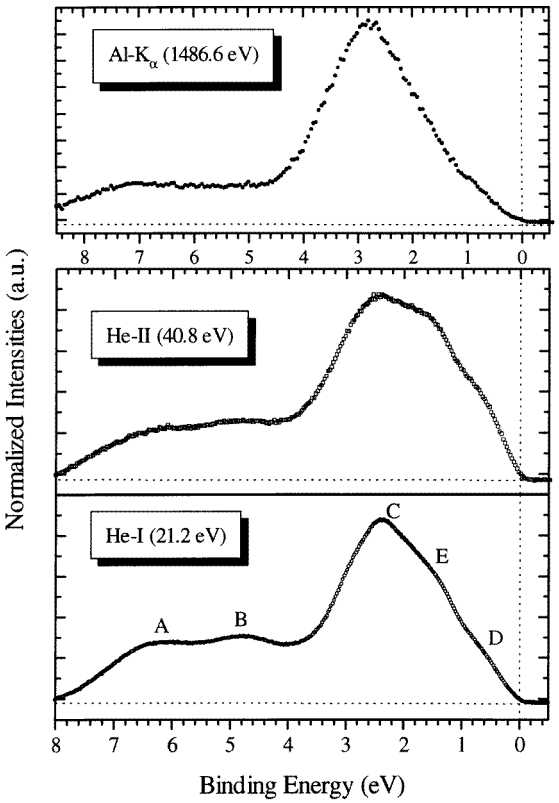

Figure 1. The XP spectrum and UP spectra of PdO in the valence band regime. The spectra were subtracted by a Tougaard background and satellite corrected (UP spectra). The XP spectrum was performed with the monochromatized source. The overall energy resolutions were 0.1, 0.2, and 0.6 eV for He-I, He-II, and Al Kα respectively.

3. Results and discussion

3.1. The valence and conduction bands of PdO

The valence band spectra of PdO are shown in figure 1 measured with He-I, He-II, and monochromatized Al Kα radiation. The He spectra are corrected for radiation satellites. All spectra are corrected for a background of inelastically scattered electrons following

the procedure of Tougaard [20] using an energy loss function obtained from our REELS experiments on the same samples. All spectra are normalized to the same area. The valence bands show five structures, labelled A–E in the following, corresponding to those given by Holl *et al* [9]. The shoulder at E is not seen in the data of Holl *et al*. As discussed below it derives from O 2p/Pd 4d hybridized states. Therefore different oxygen stoichiometries in the surface of the samples are probably responsible for these differences. The peak energies of the peaks A–D agree very well with those given in [9].

Table 2. Total photoabsorption cross sections for the relevant orbitals (taken from [21]).

Total photoabsorption cross section $\sigma(10^6$ barn) after Yeh *et al* [21]	He-I	He-II	Al Kα
Pd $4d^8$	20.84	26.016	0.0128
O $2p^6$	16.005	10.224	0.000 36
Ratio σ(Pd $4d^8$)/σ(O $2p^6$)	1.30	2.54	35.56

In order to clarify the origin of the different structures table 2 gives the total photoabsorption cross sections for He-I, He-II, and Al Kα radiation for the Pd $4d^8$ and O $2p^6$ shells obtained from the calculations for free O/Pd atoms given by Yeh *et al* [21]. From this table we notice at once that the O 2p contributions to the spectra are strongly attenuated in the XPS data, compared to the UP spectra. From the spectra one can see that the region around the peaks (E, D) and (A, B) is enhanced in the He-I–He-II spectra. That means these regions should contain most of the O 2p derived states. This is in agreement with the partial Pd 4d–O 2p density of states (PDOS) given in the LDA calculations in [8] (see also figure 2).

A detailed comparison to the LDA calculations of Park *et al* [8] is presented in figure 2. The PDOSs of the calculations are weighted by their photoabsorption cross sections for the respective photon energies. The result is convoluted with a Gaussian of 0.7 eV FWHM for XPS and 0.2 eV FWHM for He-I–He-II and the results are slightly shifted by 0.6 eV to higher binding energies. As can be seen from figure 2 these simulated spectra agree reasonably well with the experimental ones, except in the range around structure B at about 5 eV. The O 2p contributions to the electronic structure in this range seem to be too small in the theory. The unoccupied part of the band structure is shown in figure 3, which combines the XP valence band spectrum and the Bi spectrum after normalization to the same maximum intensity. The shaded areas are the total DOS from the LDA calculations of Park *et al* [8], where the unoccupied side of the DOS has been shifted by 0.6 eV away from E_F. The two structures given in the theoretical DOS between -0.5 and -2.5 eV cannot be resolved in the experiment, which has only an energy resolution of 0.8 eV. This is demonstrated in the inset of figure 3 where the DOS in the BIS has been deconvoluted by a Gaussian with 0.8 eV width. Apart from the intensity ratios of the different structures, which may probably be traced back to energy dependent cross sections, the agreement between theory and experiment is reasonable.

Since both the XPS–UPS and Bi spectra tail out to the Fermi energy it is difficult to extract a value for the energy gap. It remains unclear whether this tailing out is partially due to nonstoichiometries in the outer surface regions. By extrapolating the steepest slope in the spectra to zero intensity we can only say that the gap is somewhere between 0 and 1 eV. Former measurements give values around 1 eV [1, 7, 12, 13].

A REEL spectrum taken at 1500 eV electron energy is presented in figure 4 (lower curve). An extrapolation to the background intensity of the zero-loss line would give a

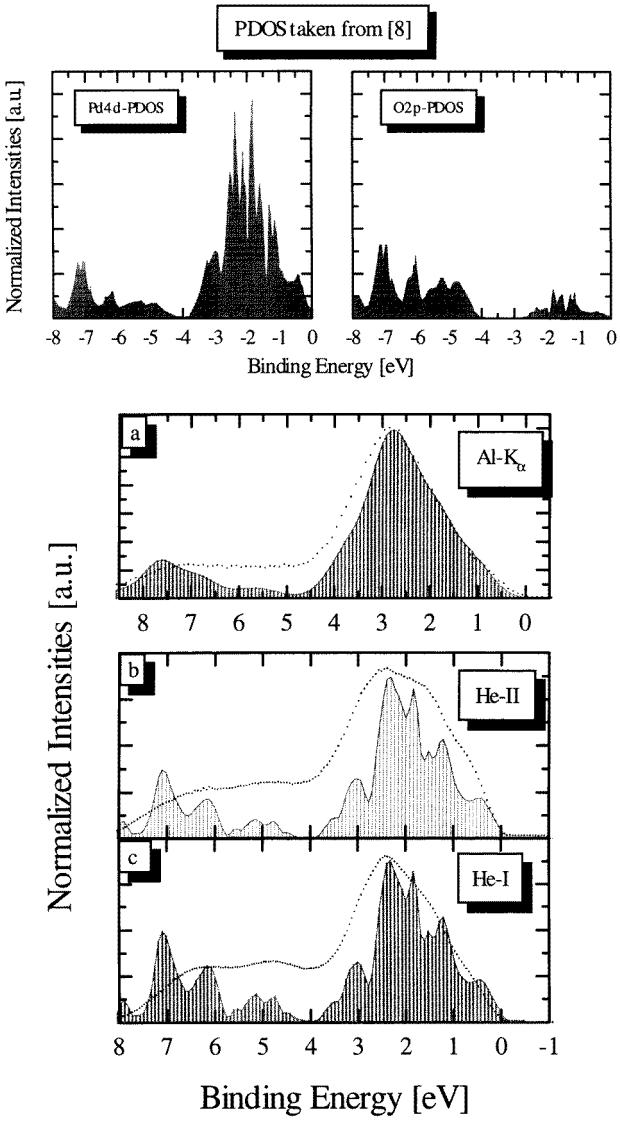

Figure 2. A comparison of our experimental data to the LDA calculation of Park *et al* [8]. At the top we show the partial densities of states (PDOSs) for the Pd 4d and O 2p orbitals taken as raw data. The three lower pictures show on the one hand our spectra again from figure 1 and on the other hand the result of the comparison. In order to obtain this we multiplied the PDOSs by the respective cross sections from table 2. After that we just added the weighted DOSs and convoluted them with Gaussians (FWHM, 0.7 eV for Al Kα, 0.2 eV for He-II and He-I) in order to take the resolution into consideration. The DOSs were shifted on the energy axis and the spectra were normalized to the maximum.

slightly larger value of about 1.5–2 eV for the gap. In figure 4 we also compare the REEL spectrum with a convolution of the BIS and the XP spectrum. This coincides in position roughly with the REEL spectrum, which means that the charge conserving excitations in REELS are roughly given by a combination of $(N-1)$ and $(N+1)$ excitation spectra,

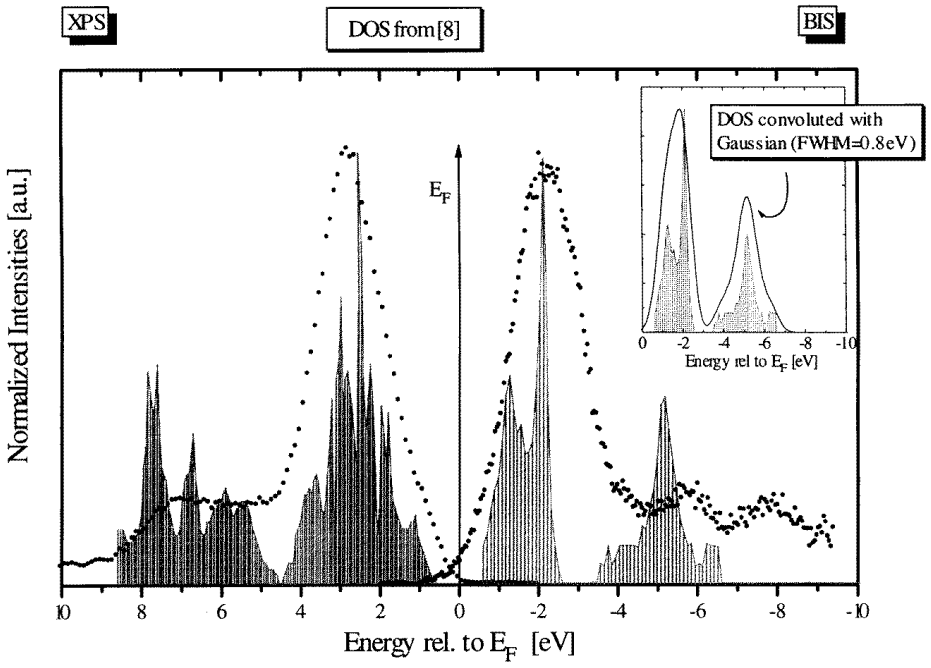

Figure 3. XP and Bi spectra of PdO referring to the Fermi edge. The XP spectrum was performed with the monochromator. The resolutions were 0.6 eV for XPS and 0.8 eV for BIS. The shaded areas again denote the DOS calculation of Park. The inset reveals the effect of a convolution of the unoccupied DOS with the resolution function for BIS, here a Gaussian with $\Gamma = 0.8$ eV.

where N denotes the electron number in the neutral ground state, which again leads to the conclusion that a single-particle picture may be a good starting point for the electronic structure of 4d TMOs, at least for PdO.

3.2. Correlation satellites

As mentioned above the photoemission spectra can rather well be explained in terms of a one-electron picture. Nevertheless correlation satellites are visible. Hence we show in figure 5 once again XP spectra of both the PdO valence band and the Pd 3d core levels. All spectra have been taken with monochromatized Al Kα radiation and were corrected for a Tougaard background. The inset in figure 5 shows the Pd 3d doublet, but now with in this case the best energy resolution of 0.5 eV in order to distinguish the features more clearly. The spectra reveal two satellites corresponding to the PdO main lines. One satellite (S1) is visible at an energy distance of about 2.65 eV, the second (S2) at a distance of about 9 eV from the Pd main line. At least S2 seems to be Pd induced because there is no similar structure 9 eV above the O 2s line. Besides one can also see this 9 eV satellite in the Pd 3p spectrum (see figure 6(b)). Because of the greater linewidths satellite S1 is not seen as a distinct feature in the other core level spectra and in the valence band.

Though the spectra have been corrected for a Tougaard background, it cannot be excluded that the satellite S1 arises from an extrinsic energy loss of the photo-electron since in the loss spectrum (figure 4) a structure is seen at approximately 2.9 eV, too, which

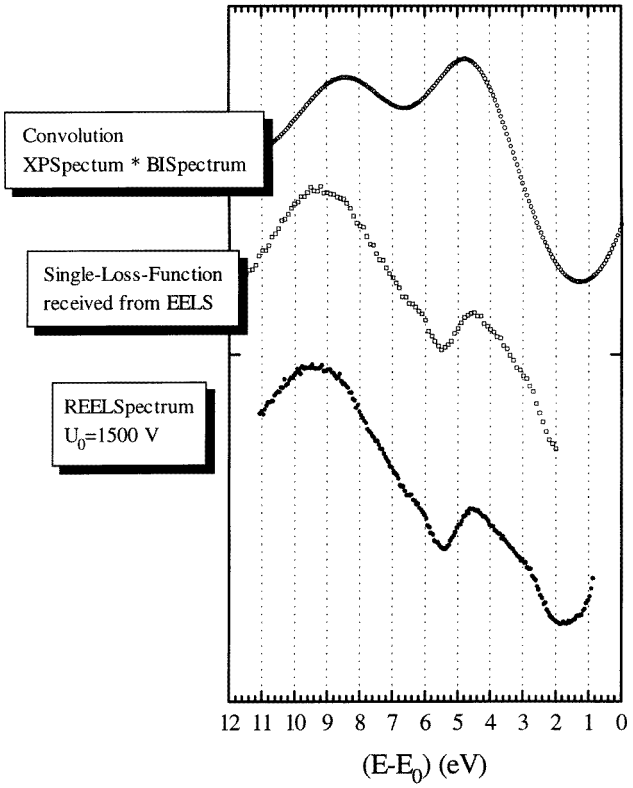

Figure 4. The upper spectrum shows the convolution of the XPS and BIS data from figure 3 compared to both the original REEL spectrum (initial energy 1500 eV) and the derived single-loss function. For survey the zero-loss line has been cut off and all spectra were normalized to the peak at 9 eV.

was formerly explained as an interband transition by Tardy *et al* [22]. This view is supported by the paper of Cox *et al* [23] showing loss features in ternary Ru oxides at energies of about 0.8–3.5 eV. On the other hand, crystal field effects and multiplet effects caused by the interaction between the 3d core hole and the unfilled Pd 4d shell which can be expressed in terms of the Slater Coulomb and exchange integrals [24] may also be a reason for the satellite structure S1 [33], although one then would expect a difference in the lineshapes of the Pd $3d_{5/2}$ and $3d_{3/2}$ deduced parts, so at the moment the origin of satellite S1 is not clear. Nevertheless its occurrence could be responsible for the discrepancy between the VB spectra and the LDA calculations around peak B in figure 1.

In order to explain the satellite S2 (which is not found in the band-structure calculation either) we performed simple cluster model calculations [25–27] for the 3d core level in the space of the basis states $4d^8$, $4d^9L^{-1}$, $4d^{10}L^{-2}$ (where L^{-1} means a hole in the O 2p shell) and obtained a series of parameter sets (Δ, U_{dd}, U_{cd}, T) which were able to adjust the experimentally found satellite intensity (6–7% with respect to the main line) and main line–satellite line energy splitting (8.5–9 eV). Whereas the charge transfer energy Δ, the 4d electron correlation energy U_{dd}, and the core hole–4d electron attraction U_{cd} cannot be fixed to definite values, the hybridization parameter T is restricted to about 3.5 eV in all cases, leading to an effective hybridization of $T_{eff} = \sqrt{n_h}T = 5$ eV. Here $n_h = 2$ is the number of holes in the Pd 4d shell for PdO in a purely ionic picture. On the other hand one

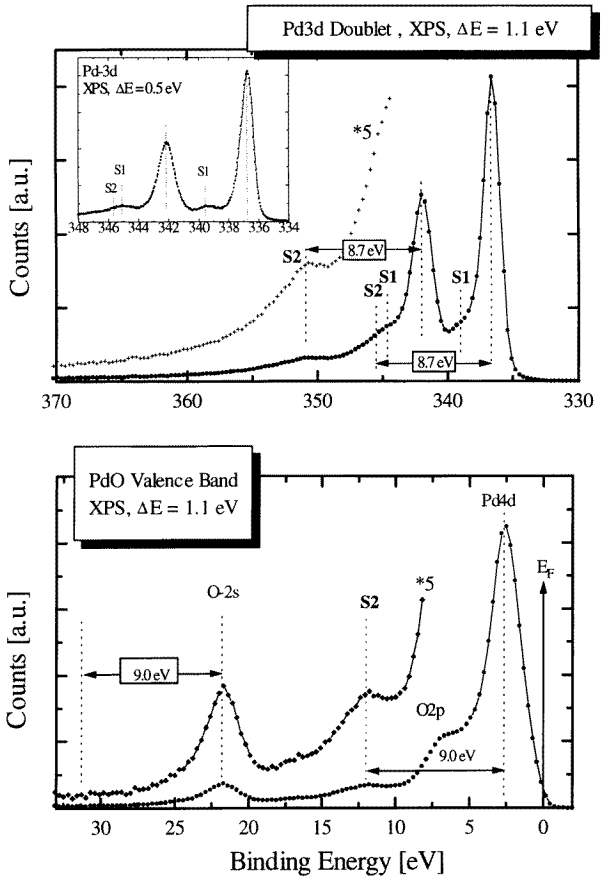

Figure 5. XP spectra of both the PdO valence band and the Pd 3d core levels. All spectra were taken with the monochromator and have been corrected for a Tougaard background. The respective energy resolutions are given. Note that in the inset the Pd 3d core level was measured with the best obtainable energy resolution.

obtains $|\Delta - U_{cd}| < 4$ eV if Δ and U_{cd} are chosen in a reasonable parameter range. Since in a two-level model the main line–satellite line splitting is given by $\sqrt{(\Delta - U_{cd})^2 + 4T_{eff}^2}$, this means that at least half of the satellite distance is caused by the hybridization effect.

This reminds us of the strong influence of the hybridization in the cluster model analysis of excitation spectra for early 3d TMOs such as TiO_2 or V_2O_3 [28–30], which in this case can be attributed to the large number n_h of 3d holes leading to a reduction of correlation. The effect of contraction of the 3d orbitals with increasing atomic number in the 3d series increases the influence of the d–d correlations in the late 3d TMOs. For example in NiO (also a d^8 system) a smaller T_{eff} of about 3 eV was found [31, 32]. In PdO the more delocalized 4d orbitals weaken the correlation compared to NiO, so the resemblance to the early 3d TMOs is understandable. Finally it should be mentioned that a cluster model analysis including the first satellite S1 did not give any reasonable results, supporting the fact that it has a different origin.

Therefore as a preliminary result we can explain satellite S2 in a screening picture by means of a charge transfer process. A good estimate especially of U_{dd} might help to

reduce the number of possible parameter sets in the cluster model to give more specific values for PdO. Resuming, the one-electron picture (ground state!) explains the valence band spectra (photoemission final state!) rather well because of the reduced influence of correlation (many-electron) effects, but satellite structures occurring in the photoemission spectra indicate that correlations may not be negligible even in 4d compounds. This point should be reexamined in more detail in the future.

Additionally we would like to stress that the term 'one-electron picture' used for the band-structure calculations does not mean that ground state correlations are not included in density-functional methods, for example LDA calculations, but that such a treatment does not intend to describe excitations in correlated systems showing up in satellite structures as seen for example in the photoemission spectra of PdO.

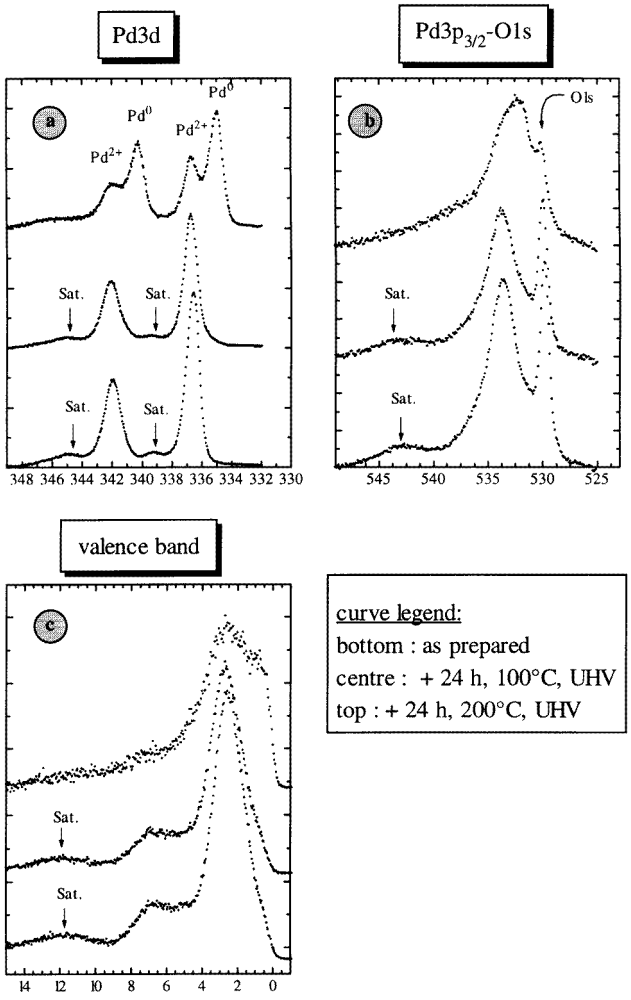

Figure 6. Monochromatized XP spectra of (a) the Pd 3d doublet, (b) the Pd $3p_{3/2}$–O 1s 'doublet', and (c) the valence band. The bottom spectra give the clean PdO sample whereas the middle and the top spectra show the sample after the two annealing procedures. Details are given in the text. All spectra are background subtracted. The arrows indicate the charge transfer satellites.

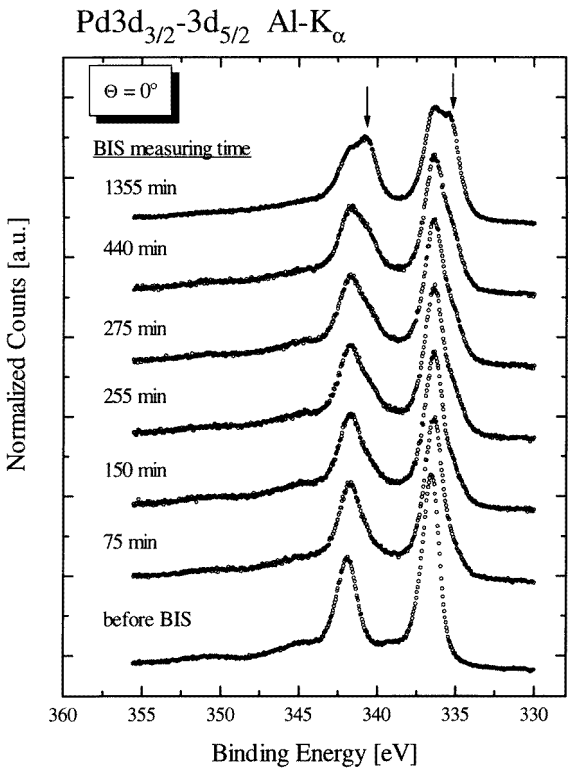

(a)

Figure 7. (a) XP spectra of the Pd 3d doublet depending on the BIS measuring time. The data were collected in this case with the twin anode so a satellite correction was carried out as well as the background subtraction. For convenience the spectra were normalized to the measuring time. (b) The same spectrum series but now for the Pd $3p_{3/2}$–O 1s 'doublet'. All other conditions remained the same as in (a). (c) BI spectra taken for the indicated measuring times. After each BIS measurement XP spectra were collected; these are shown in (a) and (b). The BIS data were normalized to the inelastic background, i.e. to the area from −6 to −9 eV binding energy.

3.3. Instability effects

Finally we report on the instability of the PdO surface observed during course of these experiments. Figure 6 shows XP spectra (measured with monochromatized Al Kα radiation and background subtracted by using the Tougaard procedure as described before), namely the Pd 3d doublet (figure 6(a)), the Pd $3p_{3/2}$ line together with the O 1s line (figure 6(b)) and the valence band (figure 6(c)) for different sample treatments. The lower curve is from PdO as prepared, followed by a 24 h anneal at 100 °C (middle curve) and by an additional 24 h anneal at 200 °C (upper curve) under UHV conditions. Annealing at 100 °C leads to a small decrease of the O 1s intensity without any significant changes in the Pd and valence band spectra. Annealing at 200 °C shows a large loss of the O 1s intensity accompanied by the appearance of an additional Pd signal close to the signal in Pd metal (for the binding energies see table 1) and the valence band shows a large increase of the intensity close to the Fermi energy accompanied by a loss in intensity of the O 2p features around 7 eV binding energy. This clearly shows that annealing of the sample at moderate temperatures already

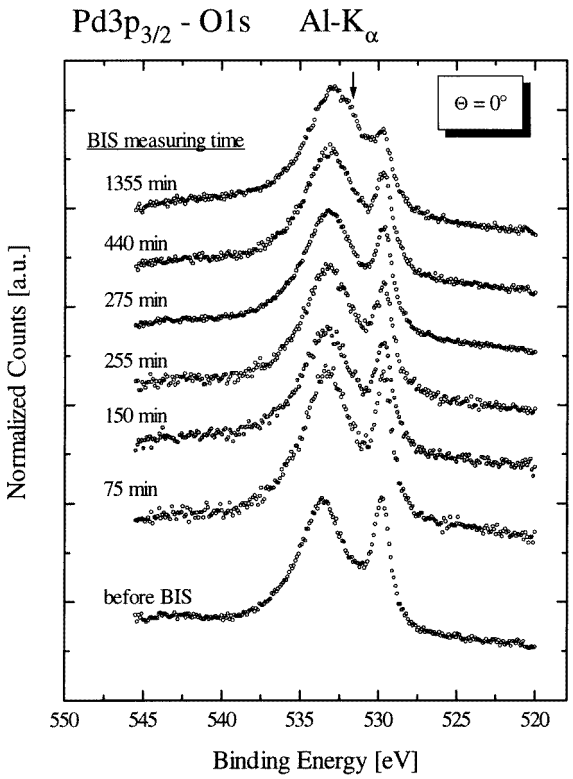

(b)

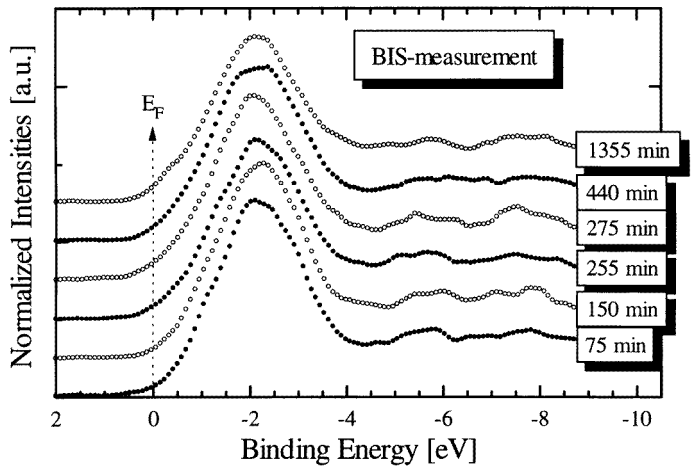

(c)

Figure 7. (Continued)

leads to a loss of oxygen in the surface region of the sample, which leads to a reduction of Pd^{2+} ($4d^8$) to a Pd-metal-like $4d^{10}$ state, giving a large density of Pd 4d states close to the Fermi energy. This behaviour of course makes it very difficult to extract reliable data for

the band gap of these spectroscopy data and may also be the reason for the scatter of the gap value given in the literature [1, 7, 12, 13].

A similar loss of oxygen has been observed during the electron bombardment in the BIS experiments. Figure 7 shows XP (in this case with the Mg Kα twin anode) and BI spectra as a function of time over about 24 h of a BIS run. Already after 2–3 h we observe a loss of oxygen and the appearance of the Pd $4d^{10}$ states. At the end of the run the oxygen loss is similar to that observed in the annealing experiments at 200 °C. In the BI spectra (figure 7(c)) we observe a continuous decrease of the ($4d^8 \rightarrow 4d^9$) transition at about -2.5 eV as compared to the background between -6 and -10 eV. No additional structure is visible close to the Fermi energy. Therefore the behaviour of the BI spectra supports the conclusions drawn from the annealing experiments that either by heat or radiation damage due to electrons the PdO surface is reduced with the creation of Pd $4d^{10}$-like species. The BI spectra reported in subsection 3.1 and discussed in connection with the band-structure calculations have therefore been obtained by adding several BI spectra measured over less than 2 h on freshly oxidized samples.

4. Conclusion and outlook

The valence and conduction band structure of PdO obtained from photoemission and inverse photoemission is in reasonable agreement with one-electron band-structure calculations. Nevertheless satellites observed in the Pd core level spectra and in the XP valence band spectra show that electron–electron interactions may not be neglected either in the interpretation of the electronic properties of the 4d TMOs. These effects should be investigated in more detail by resonant photoemission or by taking spectra at the Cooper minimum of the Pd 4d photoabsorption cross section by using tunable synchrotron radiation.

The surface of PdO is very sensitive to reduction processes. One has to be aware of these effects in the interpretation of the spectroscopic data of PdO and probably of similar systems, too.

Acknowledgments

This work was supported by the Deutsche Forschungsgemeinschaft. We would like to thank Dr H Schmitt and B Wiegand of the Department of Technical Physics for the preparation of one of our samples and R Niegisch of the group of Professor Schwitzgebel (Physical Chemistry) for the examinations of the powder pellet concerning the crystalline structure and the stoichiometry.

References

[1] Okamoto H and Aso T 1967 *Japan. J. Appl. Phys.* **6** 779
[2] Waser J 1953 *Acta. Crystallogr.* **6** 661
[3] Hüfner S 1994 *Adv. Phys.* **43** 183
[4] Orent T W and Bader S D 1982 *Surf. Sci.* **115** 323
[5] Conrad H, Ertl G, Küppers J and Latta E E 1977 *Surf. Sci.* **65** 235
[6] Hass K C and Carlsson A E 1992 *Phys. Rev.* B **46** 4246
[7] Ahuja R, Auluck S, Johansson B and Khan M A 1994 *Phys. Rev.* B **50** 2128
[8] Park K, Novikov D L, Gubanov V A and Freeman A J 1994 *Phys. Rev.* B **49** 4425
[9] Holl Y, Krill G, Amamou A, Légaré P, Hilaire L and Maire G 1979 *Solid State Commun.* **32** 1189
[10] Brandow B H 1977 *Adv. Phys.* **26** 651
[11] Goodenough J B 1971 *Progress in Solid State Chemistry* vol 5 (Oxford: Pergamon) p 145

[12] Nilsson P O and Shivaraman M S 1979 *J. Phys. C: Solid State Phys.* **12** 1423
[13] Hulliger F J 1965 *J. Phys. Chem.* **26** 639
[14] Rey E, Karmal M R, Miles R B and Royce B S H 1978 *J. Mater. Sci.* **13** 812
[15] Rogers D B, Shannon R D and Gillson J 1971 *J. Solid State Chem.* **3** 314
[16] Tura J M 1988 *Surf. Interface Anal.* **11** 447
[17] Moddemann W E and Grove D R 1988 *Surf. Interface Anal.* **11** 317
[18] Légaré P and Maire G 1989 *Surf. Sci.* **217** 167
[19] Kim K S and Winograd N 1974 *Anal. Chem.* **46** 197
[20] Tougaard S 1990 *J. Electron Spectrosc. Relat. Phenom.* **52** 243
[21] Yeh J J and Lindau I 1985 *At. Data Nucl. Data Tables* **32** 7
Yeh J J and Lindau I 1985 *At. Data Nucl. Data Tables* **32** 9
[22] Tardy M and Bozon-Verduraz F 1975 *C. R. Acad. Sci., Paris* **280** C 317
[23] Cox P A, Egdell R G, Goodenough J B, Hamnet A and Naish C C 1983 *J. Phys. C: Solid State Phys.* **16** 6221
[24] Slater J C 1960 *Quantum Theory of Atomic Structure* (New York: McGraw-Hill)
[25] van der Laan G, Westra C, Haas C and Sawatzky G A 1981 *Phys. Rev.* B **23** 4369
[26] Park J, Ryu S, Han M and Oh S-J 1988 *Phys. Rev.* B **37** 10 867
[27] Kotani A, Mizuta H, Jo T and Parlebas J C 1983 *Solid State Commun.* **53** 805
[28] Parlebas J C 1992 *J. Physique* I **61** 1369
[29] Okada K, Uozumi T and Kotani A 1994 *J. Phys. Soc. Japan* **63** 3176
[30] Bocquet A E, Mizokawa T, Morikawa K, Fujimori A, Barman S R, Maiti K, Sarma D D, Tokura Y and Onoda M 1996 *Phys. Rev.* B **53** 1161
[31] Lee G and Oh S-J 1991 *Phys. Rev.* B **43** 14 674
[32] Okada K and Kotani A 1992 *J. Phys. Soc. Japan* **61** 4619
[33] Kotani A and Uozumi T 1996 private communication